Received 30 March 2022; revised 28 May 2022 and 22 June 2022; accepted 2 July 2022.
Date of publication 8 July 2022; date of current version 18 July 2022.

Digital Object Identifier 10.1109/OJUFFC.2022.3188746

Laser Micromachined Flexible Ultrasound Line Array and Subplanar Multimodal Imaging Applications

JIANZHONG CHEN[1], WEI LIU[1], DAWEI WU[1] (Member, IEEE), AND HU YE[2]

[1]State Key Laboratory of Mechanics and Control of Mechanical Structures, Nanjing University of Aeronautics and Astronautics, Nanjing 210016, China
[2]Keya Medical, Shanghai 210000, China

CORRESPONDING AUTHORS: D. WU (dwu@nuaa.edu.cn) and H. YE (yehu2006@163.com)

This work was supported in part by the National Key Research and Development Project under Grant 2019YFE0109300 and in part by the National Natural Science Foundation of China under Grant 52075240.

ABSTRACT Flexible ultrasound array with phased array configurations have individually controllable array element emission and reception acoustic properties, however array conventional processes and array design are too complex. It is necessary to explore rapid creation methods and potential ultrasound applications for flexible arrays. In this paper, we provide a method for rapid fabrication of flexible transducers based on laser micromachining and verify the performance of the line array by multi-mode positioning imaging under curved surfaces. The proposed single-layered and double-sided conductive stretchable electrode configuration eliminated the blockage of acoustic waves,and 'island bridge' structures are compatible with array flexibility and array excitation for row addressing.The mechanical, acoustic and electrical interconnections of the array are verified.Based on the Verasonics system, the ultrasonic line array scans multiple steel column targets in multiple modalities under curved surfaces for imaging and localization.The results show that the ultrasonic line array can obtain clear visual localization images in A-scan, B-scan and E-scan poses.In addition, the artifacts in the images can be effectively suppressed by adjusting the depth of focus of E-scan and optimizing the sparse line array structure. It is verified that laser micromachining for rapid creation of flexible ultrasonic line array has potential applications in the field of localization imaging.

INDEX TERMS Laser micromachining, flexible ultrasonic line array, multi-modal scanning, ultrasonic imaging.

I. INTRODUCTION

ULTRASOUND imaging is an indispensable auxiliary method of modern medical diagnosis and its technology is widely used to visualize the interior of objects for nondestructive assessment, health monitoring, and medical diagnosis with non-invasive, high-precision, high-sensitivity and strong penetrating ability [1]–[3]. Ultrasound technology provides a unique, noninvasive *in vivo* appearance [4], [5]. Conventional ultrasound probes can achieve most contact and non-contact imaging, however, these rigid probes are incapable of solid interface contact and impossible to couple well with irregular non-planar surfaces [6], [7]. In addition, conventional ultrasound devices immobilize the object to be examined must receive diagnosis, treatment and detection in a fixed mode, limiting the usage scenarios [8].

Flexible ultrasound transducer is a technology that combines the art of flexible circuit electrical design with solid piezoelectric ceramics, which can be applied to various complex surfaces in a laminated manner in order to achieve dynamic and static Medical aids such as ultrasound diagnosis, ultrasound therapy, and ultrasound imaging have opened up functional diagnosis applications [9]–[11]. Recent research has focused on the development of ultrasound probes can be classified as: using organic piezoelectric films as transducers, embedding piezoelectric ceramic into polymer substrates, and fabricating capacitive micromachined ultrasonic transducers (CMUTs) [1]. However, polymer piezoelectric bodies, usually polyvinylidene fluoride and its copolymer films, are not suitable as transmitters due to their low electromechanical coupling coefficients, low dielectric constants, and high

dielectric losses [12]–[14]. CMUTs usually have lower electromechanical efficiency than piezoelectric ceramics due to inhomogeneities between array elements and parasitic capacitance [15], [16]. The use of d33 vibration mode, filled with resin in 1-3 composites, used to enhance longitudinal vibration polishing is a good example of achieving piezoelectric ceramics embedded in a polymer base, this method has low output rate and complicated process with high equipment requirements [17]–[19].

The above ultrasonic device fabrication process is complex and the processing is difficult. There is an urgent search for a method with high yield, easy operation, and can be rapidly created into stretchable ultrasound line array for various complex surfaces such as: skull, human tibia, and skin. Stretchable ultrasound technology is a technique that can combine both rigid ultrasound materials and carrier extension properties and integrates the whole into a compatible platform [9]. Laser micromachining techniques rapidly melt arbitrarily shaped stretchable structures, which provides new design methods for stretchable ultrasound line array that can achieve output rates of 100% ultrasound array fabrication [20]–[22].

In this paper, based on laser micromachining technology, a 10-element stretchable ultrasound line array is rapidly fabricated to demonstrate the array by multi-modal scanning surface imaging and to verify the potential application of laser micromachined created line array in the field of localization imaging. Section 2 provides the array design and laser micromachining, and characterizes the mechanical, electrical, and acoustic properties of the array, as well as the imaging displacement characteristics in multiple scanning modes. Section 3 provides a complete experimental system, including detailed experimental parameters and experimental coordinates. Section 4 presents the experimental results and analyzes the surface imaging results and error analysis of the flexible ultrasonic line array in three different scanning modes. The imaging performance of the laser micromachined rapidly created ultrasonic line array in multiple scanning modes in-plane and its potential applications in the field of localization imaging was verified.

II. DESIGN AND CHARACTERIZATION

A. ULTRASONIC LINE ARRAY DESIGN

The line array structure is shown in Fig. 1, with an 'island-bridge' structure connecting the whole device skeleton and three notches (0.9 × 0.9 mm) reserved on each island for carrying the square PZT [23], [24].AS shown in Fig. 1(a), the stretchable hinge uses a modified advanced serpentine hinge, which can effectively reduce the stress concentration in the stretching process [24], [25]. The array structure is shown in Figure 1(b), and the array process is designed. First, the polyimide film (PI) is covered with copper foil on both sides, and a 1mm square slot is laser micromachined. Then, the pre-scored PZT-8 is embedded in the slot, and a conductive silver paste layer is applied to both the top and bottom of the array. Finally, the rows of addressable electrodes are designed, the electrode wires are connected, and the single-sided circuit copper foil is peeled off. Test the flexible circuit after drying at 70° for 20 minutes. Each line array module carries three ceramic pressure point blocks (0.9 × 0.9mm, thickness 1.5mm). The thickness of the entire stretchable hinge matrix is 0.25mm, the width of the serpentine hinge is 0.2mm, and the center distance between the serpentine hinges is 0.4mm. As shown in Fig.1(c), the three PZT elements are integrated on the same island with 10 pins reserved in advance for external electrodes to provide excitation circuits. The single-layer island-bridge structure provided in this paper has the advantages of easy processing, high flexibility, and large stretchability compared with the multi-layer island-bridge structure studied in recent years [1], [26].As shown in Fig. 1(d), the ultrasonic linear array adopts three pieces of PZT-8 independently embedded in the polyimide groove to replace the whole piezoelectric ceramic. The main purpose of the linear array design is to provide multi-directional bending for the ultrasonic linear array to achieve array flexibility. The array size and the number are improved compared to the stretchable piezoelectric micro-ultrasonic transducer array proposed by Liu *et al.* [27].

B. LASER MICROMACHINING

Laser precision machining system (protolaser U3,LPKF Laser & Electronics, Switzerland) is used to micromachine the initial state of 'island-bridge' structure in polyimide film (covered with conductive copper film on both sides). The process flow is shown in Fig. 1. The design parameters of the ultrasonic line array are input to the laser micromachining system as graphical information for fast and accurate micromachining of the stretchable ultrasonic line array structure. The laser micromachining flexible array structure can realize one-time processing and has a very high processing yield. In addition, the limitations of laser processing are low, and the shape of the structure to be processed can be flexibly designed. Laser power, repetition rate, scanning times and scanning speed have important effects on the ablation depth and surface morphology of polyimide films, and then affect the tensile properties. When the power and repetition rate of the laser is overloaded, the superposition effect of laser energy and the phenomenon of excessive ablation become more and more obvious, resulting in the increase of ablation width caused by local material melting. Increasing the scanning speed can reduce the single processing time at the expense of ablation depth and small-size graphics accuracy. The repetition rate is set at 24 times and no ablation is evident in the cross section of the laser micromachined polyimide film.

C. MECHANICAL AND ACOUSTIC PROPERTIES CHARACTERIZATION

Agilent 4294A precision impedance analyzer is used to determine the resonant frequency fr and the anti-resonant frequency fa of the ultrasonic line array are 1.99 and 2.13 MHz. The bandwidth (−6 dB) of the array is ∼7.8% without

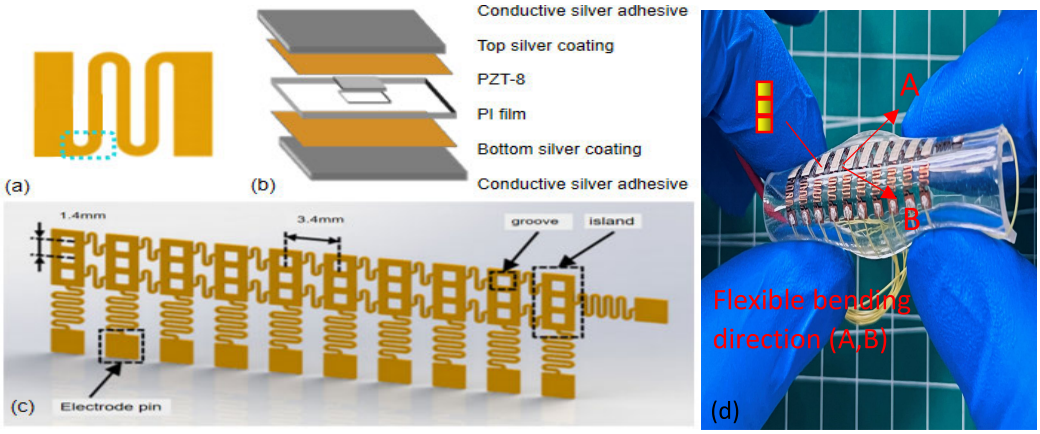

FIGURE 1. **Ultrasonic line array structure schematic.**

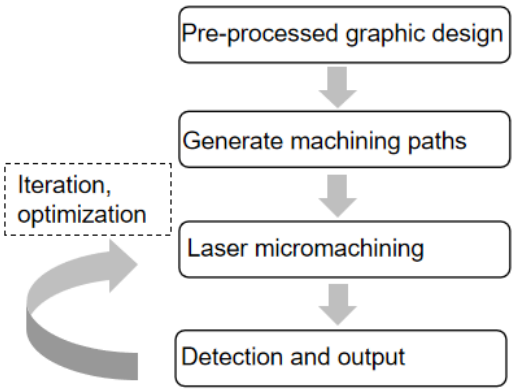

FIGURE 2. **Laser micromachining flow chart.**

matching or backing layers, and the phase angle of the transducer is about −1.7°. As shown in Fig. 3 (a) (b), the biaxial tensile test carried out on the flexible ultrasonic linear array proves that the array can obtain 100% tensile properties in both directions. The flexible adaptation of the ultrasonic line array under different stretching patterns (horizontal axis stretching, vertical axis stretching and curling) is shown in Fig. 3. The array remains in active operation under 40%-60% simultaneous biaxial stretching conditions [24], [28]. The in-mechanical properties of the array are also expressed in the fatigue resistance of the devices, and they must be able to maintain mechanical integrity during repeated loading. In addition to this, the encapsulation material can rely on its own van der Waals forces to adsorb to the surface of the body, and the flexibility can be stretched to accommodate various curves and bumps.

D. ELECTRICAL PROPERTIES CHARACTERIZATION

The electrical interconnection of the line array is through the line array single-point excitation method as shown in Fig. 4. For a 10 element line array, the lower surface of all elements is connected to the row electrodes on the lower surface of the stretchable hinge matrix, and the row electrodes are shared and grounded, with the pins noted as A. The upper surface of the elements are connected to the column electrodes on the upper surface of the stretchable hinge matrix. The upper surface of the array elements are connected to the column electrodes on the upper surface of the stretchable hinge matrix, and the column electrodes are independent of each other and not connected. The pins of 1 to 10 are correspond to 1# to 10# elements respectively. For example, when the array element 3# is to be excited, only the row electrode A and the column electrode 3 corresponding to this array element are to be excited, while the row-column electrodes corresponding to the other array elements do not form an electrical circuit and are therefore not excited. The schematic diagram of the stretchable line array with multi-point excitation is shown in Fig. 4(b).

The ultrasonic line array is interconnected by a double-sided copper film covered by a PI film, and 10+1 leads are provided outside the array for control and excitation. 10 ''row'' copper films were stripped at the top of the array to obtain individual control of the corresponding array elements by the leads, and all the ''column'' copper films were stripped at the bottom of the array. The electrodes form row and column circuit addressing in the vertical direction, and the corresponding row and column circuits can be activated through external independent leads. The active array element area is jointly determined by the selected row and column electrodes. The design of the 10+1 flexible addressing electrodes enables the array to achieve independent and ordered excitation of arbitrary cells, helping to reconstruct the shape of the target in multi-section images.

III. PHASE-CONTROLLED SCANNING

The ultrasound line array special excitation method is suitable for a variety of imaging multi-mode, type A, type B and type E imaging methods differ in the echo processing and scan path of the target. As shown in Fig. 5(b), type B scan can be regarded as a type A scan in a certain distance in a certain direction (in Fig. 5 in the direction of the X axis), which can be explained as the expansion of type A scan

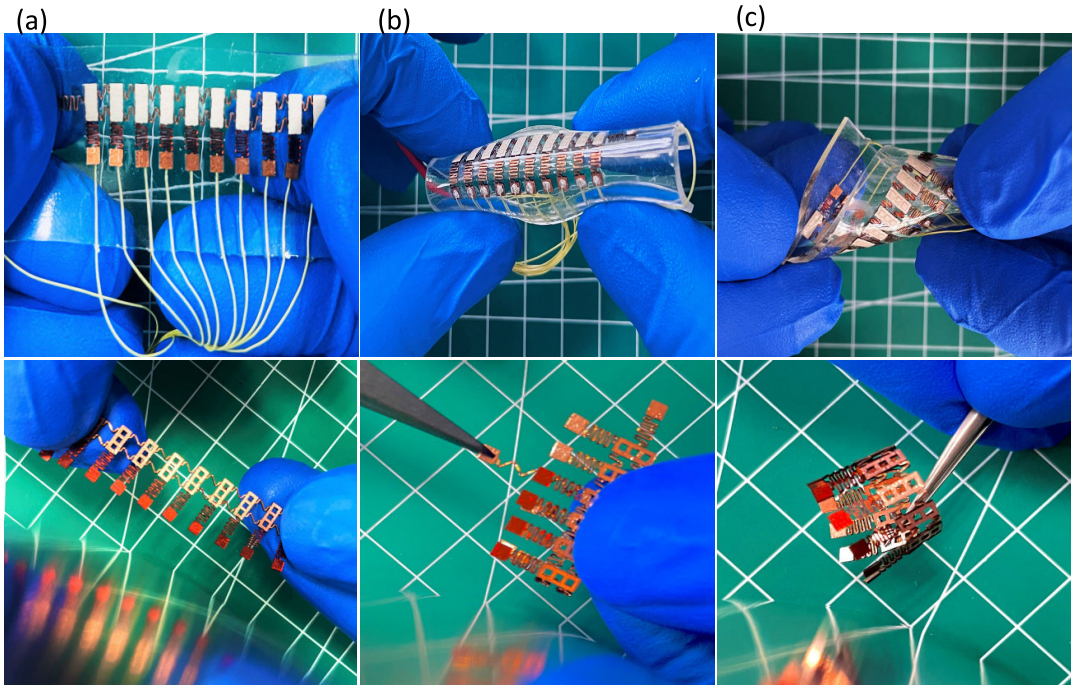

FIGURE 3. **Flexibility demonstration. (a) Extending. (b) Stretching. (c) Twisting.**

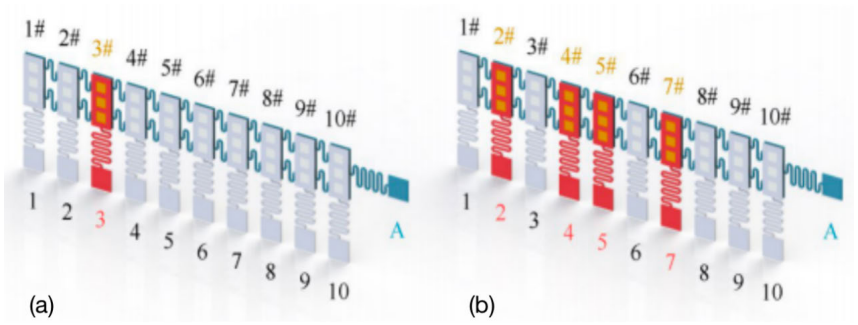

FIGURE 4. **Ultrasonic line array. (a) Single-point excitation. (b) Multi-point excitation.**

in space dimension. The scanning area is a vertical section along the X-axis direction, which has the ability to obtain two-dimensional data information in order to visually display the X and Z direction positions of the target object. The B-scan can be used for a single array or a phased array. The single array requires mechanical motion to step along the x-direction to complete multiple A-scans, and the width of the scanned longitudinal section is related to the length of the mechanical motion. The phased array can be used to excite a single element in sequence to complete an A-scan with the same position, and the width of the scan cross-section is related to the size of the phased array along the x-direction.

The E-scan is a unique scanning method of phased array, similar to the B-scan of phased array, in which the array elements are sequentially excited along the array direction to complete multiple A-scans, thus acquiring the ultrasonic data of two-dimensional cross-section, as shown in Fig. 5 (c). The E-scan of the line array requires more than one array element to participate in each scan, forming a single array element equivalent to the same aperture size, as shown in Fig. 6. Therefore, compared with the phased-array B-scan, this type of scan has higher imaging quality.

In ultrasound E-scan, the phase-controlled imaging scan is performed in a stepwise progression, where the depth of focus has an important effect on axial detection and the size of the imaging area. Z_0 denotes the natural focal length of the transducer; F_Z represents the depth of focus. According to imaging theory:

$$F_Z = Z_0 \bullet S_F^2 \left[\frac{2}{(1 + 0.5S_F)} \right] \tag{1}$$

$$S_F = {}^{F}\!/_{Z_0} \tag{2}$$

The emission aperture also plays a key factor in the imaging quality, and B_w is the width of the acoustic beam at the focal point determines the level of imaging resolution, which can be obtained from the following equation. D is the sound field diameter. A discussion of depth of focus and emission

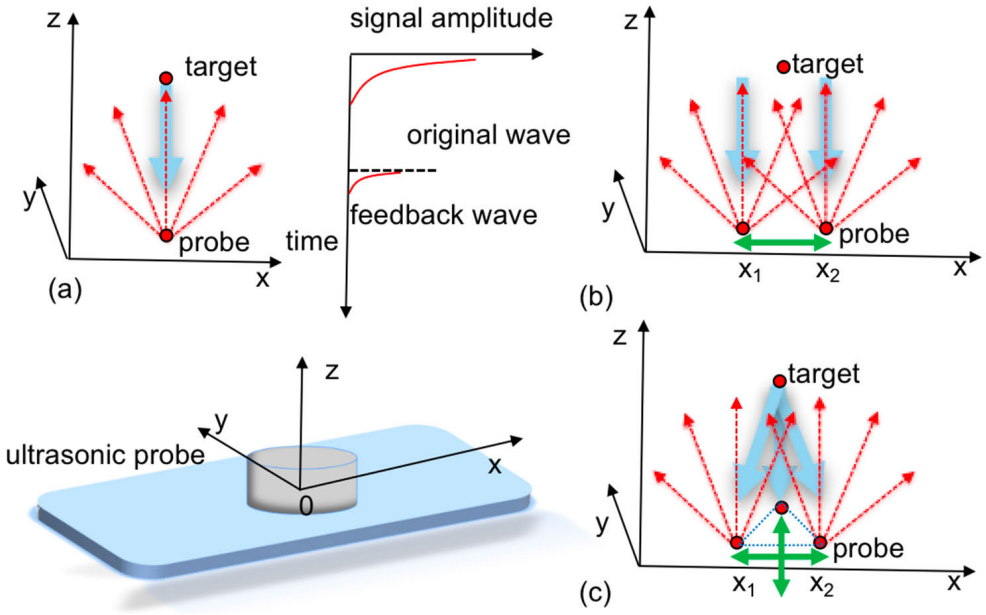

FIGURE 5. **Ultrasonic line array scan. (a) Type A. (b) Type B. (c) Type E.**

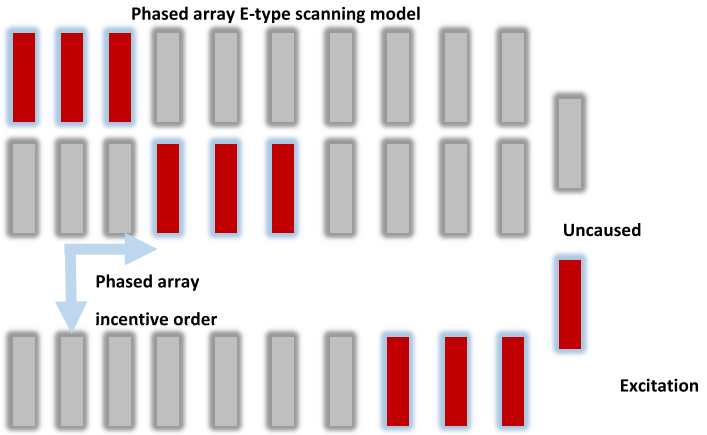

FIGURE 6. **Ultrasonic line array E-scan model.**

aperture is necessary in stretchable line array imaging.

$$B_w\,(-6dB) = 1.02f_* \bullet \lambda_m \tag{3}$$

$$f_* = {}^{F_c}/_{D} \tag{4}$$

where λ_m is sound wave in the medium wavelength; f_* is the transducer emission aperture.

As shown in Fig.7, the E-scan divides the two-dimensional imaging section into 10 columns of pixel areas, each column corresponds to 1∼10# array elements, and the emission events correspond to the array element numbers.The transmit aperture P.numTx is when the nth array element transmits, P.numTx /2 array elements on both sides transmit simultaneously. The focal depth P.txFocus is the focal depth of the sound wave emitted by the stimulated array element. The 1# array element and the P.numTx/2 array elements on the right participate in the emission, and the result obtained is placed in the first column of the imaging section in the first launch. When the number of array elements on the left side of the 2# array element is s < P.numTx, there are s array elements participating in the transmission; if s >P.numTx, there are P.numTx /2 array elements participating in the emission. There are P.numTx /2 array elements on the right side of 2# participating in the second launch. The firing events and so on complete 10 firing events and fill the imaging section with column pixels.

IV. IMAGING EXPERIMENT SYSTEM

The experimental system is shown in Fig. 8, The flexible ultrasonic line array is affixed to the curved water tank, and three steel columns are placed randomly as targets. Line array electrode wires are connected to (LEMO) connectors to build stretchable ultrasound probes that can be integrated with ultrasound imaging systems and used independently. The 10 column electrodes of the line array are used as signal

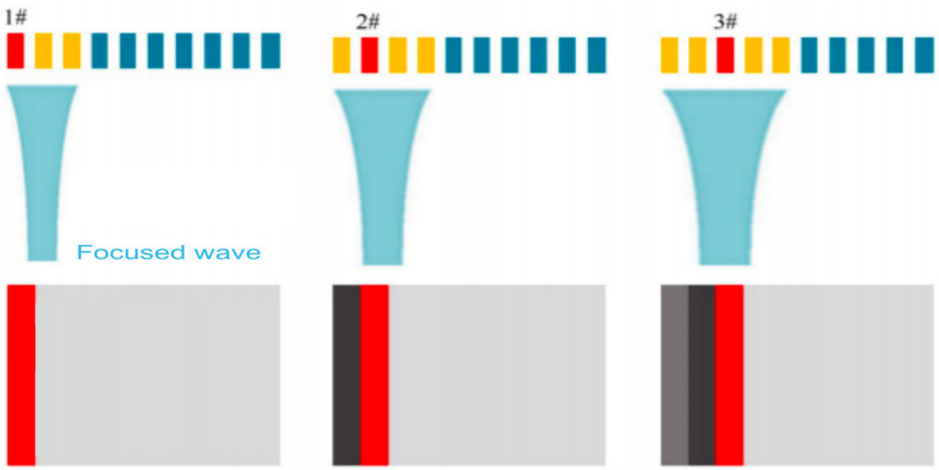

FIGURE 7. **Schematic diagram of E-scan array element launch.**

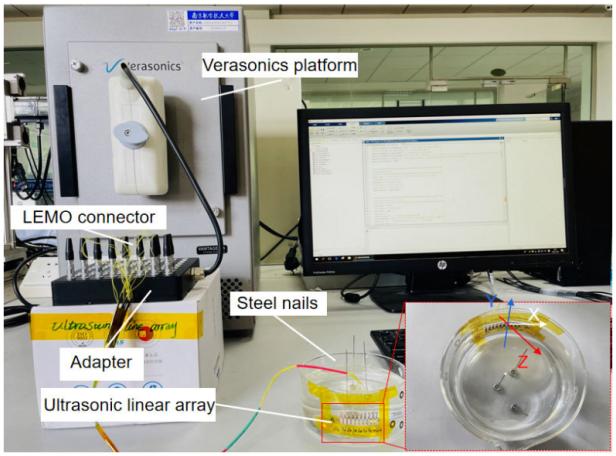

FIGURE 8. **Ultrasonic line array imaging and positioning experimental system.**

poles, corresponding to each of the 10 array elements connected directly to the signal terminal of the LEMO. The line electrodes serve all the elements as ground poles. The key parameters of the probe are shown in Tab. 1.

The 10-array stretchable ultrasound line array performs ultrasound scanning in A-type, B-type, and E-type scanning modes to capture the position of the target object based on the Verasonics system(Vantage 64 LE, Verasonics, USA) in an imaging manner. The ultrasound line array is attached to the side wall of a water tank (acoustic impedance of water is about 1.5 MRayl and soft tissue acoustic impedance is about 1.6 MRayl), and the electrode wires of the line array are connected to the adapter of the ultrasound platform panel interface through LEMO. Three 1 mm diameter steel columns are randomly placed in the flume as target objects. The target objects are distributed non-coplanar and at distances of 43 mm, 87 mm, and 132 mm from the line array.

The parameters of the ultrasound probe are defined in MATLAB. According to the imaging theory, because of the interference of the acoustic field when the array elements are distributed equidistant will cause the array acoustic field to appear as a grid flap at a particular angle, the array element pitch must be defined [29], [30]. The actual array element pitch of the ultrasonic line array is determined by optical microscopy, as shown in Tab. 2.

The theoretical pitch of the line array is 3.4 mm, and the average pitch of the actual array elements is 3.4015 mm with a polar deviation of 0.002 mm and a standard deviation of 0.073%, which can be approximated as an equally spaced arrangement. The center of the array is set as the coordinate origin, and the coordinates of each array element are shown in Tab. 3. The operating frequency is set to 2 MHz, the operating bandwidth is 1.9 ∼ 2.1 MHz, and the excitation voltage is set to 100 Vpp.

V. RESULTS AND DISCUSSION

The results of the A-scan are shown in Fig. 9, and the ultrasound data received in channel 5# corresponds to the 5th array element along the x-direction. All targets produced distinct echoes, and the echo signal amplitude became progressively smaller as the distance became larger.

$$L = {(t_w \bullet v_w)}/{2} \tag{5}$$

Equation (5) provides a linear relationship between the speed of sound and the propagation distance, t_w is the time interval, v_w is the speed of propagation of sound waves in water. The times corresponding to the maximum peak-to-peak of all target echo signals are captured with time intervals of 57.23, 114.15, and 175.02, respectively. The actual distances from the three steel columns to the surface of the line array are calculated as 42.9mm, 85.6mm, and 131.3mm. The theoretical pitches from the steel columns to the line array are 43mm, 87mm, and 132mm with a minimum error of 16%, and it matches well with the preset values. However, the A-scan is based on a simple pulse-echo principle, and the target position obtained from the imaging results is not intuitive.

The B-scan imaging scans of the ultrasonic line array need to be acquired computationally to be provided in

TABLE 1. Ultrasonic line array probe parameters.

Probe name	number	frequency（MHz）bandwidth	Array element distance
linear array	10	1.97 8.8%	3.4

TABLE 2. Ultrasonic line array actual array element pitch.

Location number	1	2	3	4	5	6	7	8	9
Numerical value (mm)	3.403	3.402	3.401	3.401	3.402	3.401	3.401	3.402	3.401

TABLE 3. Coordinates of line array elements.

Array number	1	2	3	4	5	6	7	8	9	10
x (mm)	-15.3	-11.90	-8.50	-5.10	-1.70	1.70	5.10	8.50	11.90	15.30

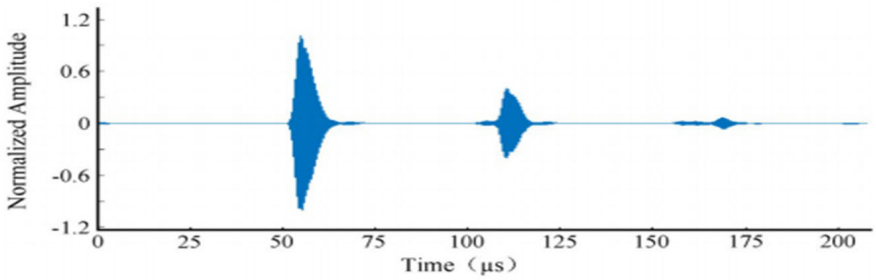

FIGURE 9. Ultrasonic line array A-scan results.

two-dimensional imaging, and the experimental results are shown in Fig. 10(a). Based on the Verasonics system, the B-scan image of the 10-array line array is more visualized than the A-scan. In Fig. 10(a), the white bright spots distributed on the vertical axis represent the position of the target in the water tank, and the vertical coordinate values of the bright spots directly correspond to the distance between the steel column and the surface of the line array. Around the bright spot of the first steel column, several bright spots with slightly darker luminance are also present. This is an artifact caused by the grid flap at a closer distance due to the array element pitch being greater than one wavelength. The other two steel columns also show artifacts, but due to the distance between the steel columns and the line array, the artifacts appear outside the imaged 2D cross section.

Fig. 10 easily shows that each E-type scan-based image quality is superior to that of the B-type scan, as evidenced by the brighter imaging points and higher resolution of the steel columns imaged in the images. In addition, the artifacts generated by the B-scan are not clearly presented in the E-scan images, indicating that the E-scan has significantly suppressed the artifacts around the first steel column. Fig. 10(b),(c),(d) shows the three imaging results of the line array under E-type scan, respectively. According to the imaging theory, we provide the imaging results under different depth of focus $P.txFocus = 100\lambda, 120\lambda$ and emitting aperture $P.numTx = 4, 6$ conditions to explore the effects of the parameters on the imaging quality.

Increasing the depth of focus($P.txFocus$) from 100λ to 120λ yields the imaging positioning results in Fig.10(b) and (c). The comparison shows that when $P.txFocus$ is increased to 120λ, the artifacts near the first steel column are further suppressed, and the size of the artifacts is slightly reduced and the brightness is also slightly diminished. However, further increase $P.txFocus$ does not improve the image quality significantly. Fig. 10(d) and (c) show the imaging results for $P.numTx = 4$ and $P.numTx = 6$, which indicates that the addition of $P.numTx$ does not significantly improve the image quality further. This is due to the fact that the total number of line array elements is small and the spacing between the elements is large, so the enhancement of the image by increasing $P.numTx$ and the deterioration of the image by the large array element spacing cancel each other

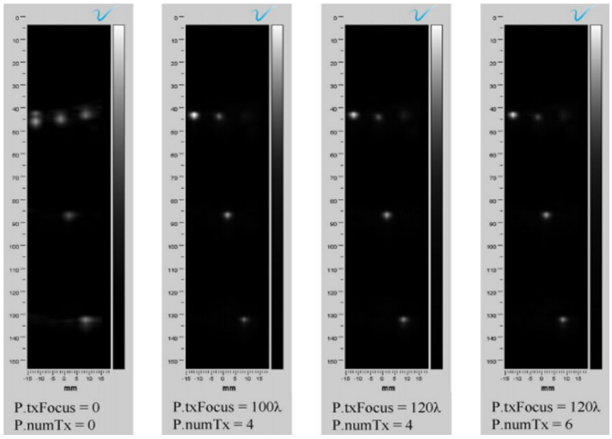

(a) B-scan (b) E-scan 1 (c) E-scan 2 (d) E-scan 3

FIGURE 10. Imaging junction of ultrasonic line array B and E scans.

out, resulting in a less significant enhancement of the imaging positioning results.

Comparing the imaging of ultrasonic linear array in different scanning modes, it can be seen that good imaging effect can be obtained under both A-scan and B-scan. Under E-scan, the ultrasonic linear array can achieve good positioning and imaging by modulating parameters, and there is an optimal depth of focus in linear electronic scanning imaging, which can achieve the highest level of imaging quality. The sparse array imaging of the line array can improve the imaging quality by adjusting the emission aperture and the pitch matching of the array elements, and this also indicates a direction for the structural optimization of the future stretchable and stretchable ultrasonic line array.

VI. CONCLUSION

This paper provides stretchable stretchable line array that are rapidly fabricated based on laser micromachining and have row-addressable electrical interconnections. The stretchable ultrasound line array is based on Verasonics for multi-modal imaging of multiple targets. Comparative analysis of the line array in type A, type B and type E scans imaging results are concluded as follows:

1 Rapidly created ultrasonic line array based on laser micromachining has the ability to achieve surface localization imaging in multiple scanning modes (A-scan, B-scan, and E-scan), validating its potential application in the field of positional imaging.

2 Excellent phase-controlled imaging can be achieved under E-scan, and the imaging quality can be improved by adjusting the depth of focus to effectively suppress imaging artifacts. In addition, there exists a best quality *P.txFocus* to improve the resolution of column array imaging and adjust the imaging artifacts.

3 The optimization ability of the emission aperture in sparse array imaging is offset by the array element spacing, and optimizing the line array structure can provide new ideas for optimal imaging of sparse arrays.

REFERENCES

[1] H. Hu *et al.*, "Stretchable ultrasonic transducer arrays for three-dimensional imaging on complex surfaces," *Sci. Adv.*, vol. 4, no. 3, Mar. 2018, Art. no. eaar3979.
[2] A. Guemes, N. Salowitz, and F. K. Chang, "Trends on research in structural health monitoring," *Struct. Health Monit. Int. J.*, vol. 13, no. 6, pp. 579–580, 2014.
[3] M. J. S. Lowe, D. N. Alleyne, and P. Cawley, "Defect detection in pipes using guided waves," *Ultrasonics*, vol. 36, nos. 1–5, pp. 147–154, 1998.
[4] M. D. Menz, Ö. Oralkan, P. T. Khuri-Yakub, and S. A. Baccus, "Precise neural stimulation in the retina using focused ultrasound," *J. Neurosci.*, vol. 33, no. 10, pp. 4550–4560, 2013.
[5] M. S. Afzal, H. Shim, and Y. Roh, "Design of a piezoelectric multilayered structure for ultrasound sensors using the equivalent circuit method," *Sensors*, vol. 18, no. 12, p. 4491, Dec. 2018.
[6] O. Casula *et al.*, "Control of complex components with smart flexible phased arrays," *AIP Conf. Amer. Inst. Phys.*, vol. 820, no. 1, pp. 829–836, 2006.
[7] F. Giovagnorio, C. Andreoli, and M. L. D. Cicco, "Color Doppler sonography of focal lesions of the skin and subcutaneous tissue," *J. Ultrasound Med.*, vol. 18, no. 2, pp. 89–93, Feb. 1999.
[8] C. Seok *et al.*, "A sub-millimeter lateral resolution ultrasonic beamforming system for brain stimulation in behaving animals," in *Proc. 41st Annu. Int. Conf. IEEE Eng. Med. Biol. Soc. (EMBC)*, Jul. 2019, pp. 6462–6465.
[9] X. Ma *et al.*, "Lead-free ultrasonic phased array transducer for human heart imaging," *IEEE Trans. Ultrason., Ferroelectr., Freq. Control*, vol. 69, no. 2, pp. 751–760, Feb. 2022.
[10] Z. Wang *et al.*, "A flexible ultrasound transducer array with micromachined bulk PZT," *Sensors*, vol. 15, no. 2, pp. 2538–2547, 2015.
[11] K. Baeg and J. Lee, "Flexible electronic systems on plastic substrates and textiles for smart wearable technologies," *Adv. Mater. Technol.*, vol. 5, no. 7, Jul. 2020, Art. no. 2000071.
[12] D. J. Powell and G. Hayward, "Flexible ultrasonic transducer arrays for nondestructive evaluation applications. I. The theoretical modeling approach," *IEEE Trans. Ultrason., Ferroelectr., Freq. Control*, vol. 43, no. 3, pp. 385–392, May 1996.
[13] Y. Qi, N. T. Jafferis, K. Lyons, C. M. Lee, H. Ahmad, and M. C. McAlpine, "Piezoelectric ribbons printed onto rubber for flexible energy conversion," *Nano Lett.*, vol. 10, no. 2, pp. 524–528, 2010.
[14] G. Harvey, A. Gachagan, J. W. Mackersie, T. Mccunnie, and R. Banks, "Flexible ultrasonic transducers incorporating piezoelectric fibres," *IEEE Trans. Ultrason., Ferroelectr., Freq. Control*, vol. 56, no. 9, pp. 1999–2009, Sep. 2009.
[15] R. S. Singh *et al.*, Eds., *Acoustical Imaging*. Cham, Switzerland: Springer, 2007, pp. 211–214.
[16] D. Certon, F. Teston, and F. Patat, "A finite difference model for cMUT devices," *IEEE Trans. Ultrason., Ferroelectr., Freq. Control*, vol. 52, no. 12, pp. 2199–2210, Dec. 2005.
[17] X. Gu *et al.*, "Temperature-dependent properties of a 1–3 connectivity piezoelectric ceramic-polymer composite," *Energy Harvesting Syst.*, vol. 2, nos. 3–4, pp. 107–112, 2015.
[18] R. Sun, L. Wang, Y. Zhang, and C. Zhong, "Characterization of 1–3 piezoelectric composite with a 3-tier polymer structure," *Materials*, vol. 13, no. 2, p. 397, Jan. 2020.
[19] J. Wang, C. Zhong, S. Hao, and L. Wang, "Design and properties analysis of novel modified 1–3 piezoelectric composite," *Materials*, vol. 14, no. 7, p. 1749, Apr. 2021.
[20] M. L. Marchoubeh *et al.*, "Miniaturized probe on polymer SU-8 with array of individually addressable microelectrodes for electrochemical analysis in neural and other biological tissues," *Anal. Bioanal. Chem.*, vol. 413, no. 27, pp. 6777–6791, Nov. 2021.
[21] Z. Y. A. Al-Shibaany, P. Penchev, J. Hedley, and S. Dimov, "Laser micromachining of lithium niobate-based resonant sensors towards medical devices applications," *Sensors*, vol. 20, no. 8, p. 2206, Apr. 2020.
[22] W. Liu and D. Wu, "Low temperature adhesive bonding-based fabrication of an air-borne flexible piezoelectric micromachined ultrasonic transducer," *Sensors*, vol. 20, no. 11, p. 3333, Jun. 2020.
[23] W. Liu, C. Zhu, and D. Wu, "Flexible piezoelectric micro ultrasonic transducer array integrated on various flexible substrates," *Sens. Actuators A, Phys.*, vol. 317, Jan. 2021, Art. no. 112476.
[24] W. Liu, W. Chen, C. Zhu, and D. Wu, "Design and micromachining of a stretchable two-dimensional ultrasonic array," *Micro Nano Eng.*, vol. 13, Nov. 2021, Art. no. 100096.

[25] W. Liu *et al.*, "Flexible piezoelectric micro ultrasonic transducer based on a laser processed substrate," in *Proc. IEEE Int. Ultrason. Symp. (IUS)*, Sep. 2020, pp. 1–4.
[26] A. M. V. Mohan *et al.*, "Merging of thin- and thick-film fabrication technologies: Toward soft stretchable 'island–bridge' devices," *Adv. Mater. Technol.*, vol. 2, no. 4, Apr. 2017, Art. no. 1600284.
[27] H. Liu *et al.*, "Flexible ultrasonic transducer array with bulk PZT for adjuvant treatment of bone injury," *Sensors*, vol. 20, no. 1, p. 86, Dec. 2019.
[28] W. Liu, C. Zhu, and D. Wu, "Flexible and stretchable ultrasonic transducer array conformed to complex surfaces," *IEEE Electron Device Lett.*, vol. 42, no. 2, pp. 240–243, Feb. 2021.
[29] L. I. U. Wei *et al.*, "Stretchable ultrasonic linear array based on laser processing," in *Proc. 15th Symp. Piezoelectrcity, Acoustic Waves Device Appl. (SPAWDA)*, Apr. 2021, pp. 35–38.
[30] T. L. Szabo, *Diagnostic Ultrasound Imaging: Inside Out*. New York, NY, USA: Academic, 2004.

JIANZHONG CHEN received the M.S. degree in mechanical engineering from the Changchun University of Technology in 2021. He is currently pursuing the Ph.D. degree with the State Key Laboratory of Mechanics and Control of Mechanical Structures, Nanjing University of Aeronautics and Astronautics, Nanjing. His current research interest topics are acoustic finite element simulation, precision machining, ultrasound imaging, and flexible ultrasound arrays.

WEI LIU received the B.S. degree (Hons.) in mechanical engineering from the Henan University of Technology, Zhengzhou, China, in 2017. He is currently pursuing the Ph.D. degree with the State Key Laboratory of Mechanics and Control of Mechanical Structure, Nanjing University of Aeronautics and Astronautics, Nanjing, China. His current research interests include acoustic finite element simulation, precision machining, and MEMS ultrasonic sensors.

DAWEI WU (Member, IEEE) received the B.S. degree from Shanghai Jiao Tong University, Shanghai, China, in 1999, the M.S. degree from the University of Miami, Coral Gables, FL, USA, in 2004, and the Ph.D. degree from the University of Southern California, Los Angeles, CA, USA, in 2009, all in biomedical engineering. He was a Senior Research Scientist with the Industrial Research of Crown Research Institutes, Wellington, New Zealand, from 2009 to 2016. In 2016, he joined the Nanjing University of Aeronautics and Astronautics, Jiangsu, China, where he is a Professor with the State Key Laboratory of Mechanics and Control of Mechanical Structures and the Director of the Institute of Precision Drive and Control. He has authored over 100 scientific publications. His current research interests include ultrasound imaging, ultrasound transducers, piezoelectric motors, and precision drive systems. He is the Deputy Editor-in-Chief of the *Journal of Vibration, Measurement and Diagnosis* and a Corresponding Expert of the *Engineering* journal of the Chinese Academy of Engineering.

HU YE, photograph and biography not available at the time of publication.